Wntless functions in mature osteoblasts to regulate bone mass

Zhendong Zhong[a,b], Cassandra R. Zylstra-Diegel[a,b], Cassie A. Schumacher[a,b], Jacob J. Baker[a,b], April C. Carpenter[c,d], Sujata Rao[c,d], Wei Yao[e], Min Guan[e], Jill A. Helms[f], Nancy E. Lane[e], Richard A. Lang[c,d], and Bart O. Williams[a,b,1]

[a]Center for Skeletal Disease Research and [b]Laboratory of Cell Signaling and Carcinogenesis, Van Andel Research Institute, Grand Rapids, MI 49503; [c]Visual Systems Group, Divisions of Pediatric Ophthalmology and Developmental Biology, Cincinnati Children's Hospital Medical Center, Cincinnati, OH 45229; [d]Department of Ophthalmology, University of Cincinnati, Cincinnati, OH 45229; [e]Center for Healthy Aging, Department of Internal Medicine, University of California at Davis Medical Center, Sacramento, CA 95817; and [f]Division of Plastic and Reconstructive Surgery, Department of Surgery, Stanford School of Medicine, Stanford, CA 94305

Edited by John T. Potts, Massachusetts General Hospital, Charlestown, MA, and approved June 4, 2012 (received for review December 12, 2011)

Recent genome-wide association studies of individuals of Asian and European descent have found that SNPs located within the genomic region (1p31.3) encoding the Wntless (Wls)/Gpr177 protein are associated significantly with reduced bone mineral density. Wls/Gpr177 is a newly identified chaperone protein that specifically escorts Wnt ligands for secretion. Given the strong functional association between the Wnt signaling pathways and bone development and homeostasis, we generated osteoblast-specific Wls-deficient (*Ocn-Cre;Wls-flox*) mice. Homozygous conditional knockout animals were born at a normal Mendelian frequency. Whole-body dual-energy X-ray absorptiometry scanning revealed that bone-mass accrual was significantly inhibited in homozygotes as early as 20 d of age. These homozygotes had spontaneous fractures and a high frequency of premature lethality at around 2 mo of age. Microcomputed tomography analysis and histomorphometric data revealed a dramatic reduction of both trabecular and cortical bone mass in homozygous mutants. Bone formation in homozygotes was severely impaired, but no obvious phenotypic change was observed in mice heterozygous for the conditional deletion. In vitro studies showed that *Wls*-deficient osteoblasts had a defect in differentiation and mineralization, with significant reductions in the expression of key osteoblast differentiation regulators. In summary, these results reveal a surprising and crucial role of osteoblast-secreted Wnt ligands in bone-mass accrual.

Osteoporosis is a bone disease characterized by a significant loss of bone mass, resulting in an increased risk of fracture. In the United States alone, more than 40 million people have osteoporosis or are at high risk of developing it. During the past decade, analysis of families with severe bone disorders (such as sclerosteosis, osteoporosis-pseudoglioma syndrome, and high-bone-mass syndrome) has identified key genes related to bone development and homeostasis (1–3). More recently, genome-wide association studies have identified additional genomic regions in which SNPs are associated with reduced bone mineral density (4–7). Two SNPs strongly associated with reduced bone mass were identified within an intron of the human *Gpr177* gene (5, 7). Wntless (Wls, also known as "Gpr177," "Evenness Interrupted," or "Sprinter") is evolutionarily conserved from worms to humans (8, 9) and is required for the normal secretion of Wnt ligands from cells (8, 10, 11). Wls is highly specific for Wnt secretion, and, to date, Wnt-independent functions have not been reported. Underscoring the importance of Wls in Wnt signaling and normal development, mice homozygous for a germline-inactivating mutation in *Wls* die early in embryonic development with defects in the embryonic axis (10).

Wnt/β-catenin signaling plays an important role in bone development and metabolism by controlling both bone formation and resorption. Studies of genetically engineered mice have shown that downstream effector molecules (such as β-catenin) in the canonical Wnt pathway, as well as endogenous inhibitors of Wnt signaling such as Dkk1 and sclerostin, have profound regulatory roles in bone cells. In the adult mouse skeleton, multiple Wnts are expressed in osteocytes, chondrocytes, and bone marrow cells (12). In addition, osteoclasts can secrete Wnt ligands to stimulate osteoblast differentiation, potentially linking bone formation and resorption (13). However, which cell type(s) in the bone microenvironment produce Wnt ligands important for normal bone development and homeostasis has yet to be determined. Because the vertebrate Wnt family consists of 19 members, it is impractical to delete all family members simultaneously from a specific cell type to resolve this question.

In this study, we conditionally inactivated *Wls* in mature osteoblasts using Cre recombinase driven by the osteocalcin promoter (*Ocn-Cre*) and, as a consequence, blocked the secretion of all Wnts from mature osteoblasts and osteocytes. Mice homozygous for the conditional deletion of the *Wls* gene in mature osteoblasts developed a severe low-bone-mass phenotype resulting from both decreased bone formation and increased matrix resorption. Our results establish two important concepts. First, the function of Wls within mature osteoblasts may explain why genetic alterations in this genomic region associate with low bone mineral density in humans. Second, our data suggest that Wnts secreted specifically from mature osteoblasts are necessary for normal bone-mass accrual in adults.

Results

Generation of Osteoblast-Specific Wls-Deficient Mice. As a first step in determining whether mature osteoblasts are a source of Wnts in the bone microenvironment, we used RT-PCR to determine which Wnt genes are expressed by primary osteoblasts. Analyzing cDNAs from calvarial cells of 3-d-old neonatal mice, we found expression of Wnt 2, 4, 5a, 10b, 11, and 16 (Fig. S1*A*). This pattern is similar to that seen in human mesenchymal stem cells from the femoral head (14). The transcription of genes for Wnt2, 4, 10b, and 11 (but not Wnt5a or 16) increased as osteoblast differentiation progressed (Fig. 1*A*). Having observed that Wnts are expressed in mature osteoblasts, we decided to define further their physiological significance and the function of the *Wls* gene by creating mice carrying a conditional deletion of *Wls* in mature osteoblasts. A previously described conditional allele of *Wls* (15) was crossed to a strain expressing Cre recombinase in mature osteoblasts (*Ocn-Cre*) (Fig. 1*B*) to generate offspring with *Wls*

Author contributions: Z.Z., J.A.H., and B.O.W. designed research; Z.Z., C.R.Z.-D., C.A.S., J.J.B., and M.G. performed research; A.C.C., S.R., and R.A.L. contributed new reagents/analytic tools; Z.Z., W.Y., J.A.H., N.E.L., and B.O.W. analyzed data; and Z.Z. and B.O.W. wrote the paper.

The authors declare no conflict of interest.

This article is a PNAS Direct Submission.

[1]To whom correspondence should be addressed. E-mail: bart.williams@vai.org.

See Author Summary on page 13146 (volume 109, number 33).

This article contains supporting information online at www.pnas.org/lookup/suppl/doi:10.1073/pnas.1120407109/-/DCSupplemental.

Downloaded at Palestinian Territory, occupied on November 26, 2021

www.manaraa.com

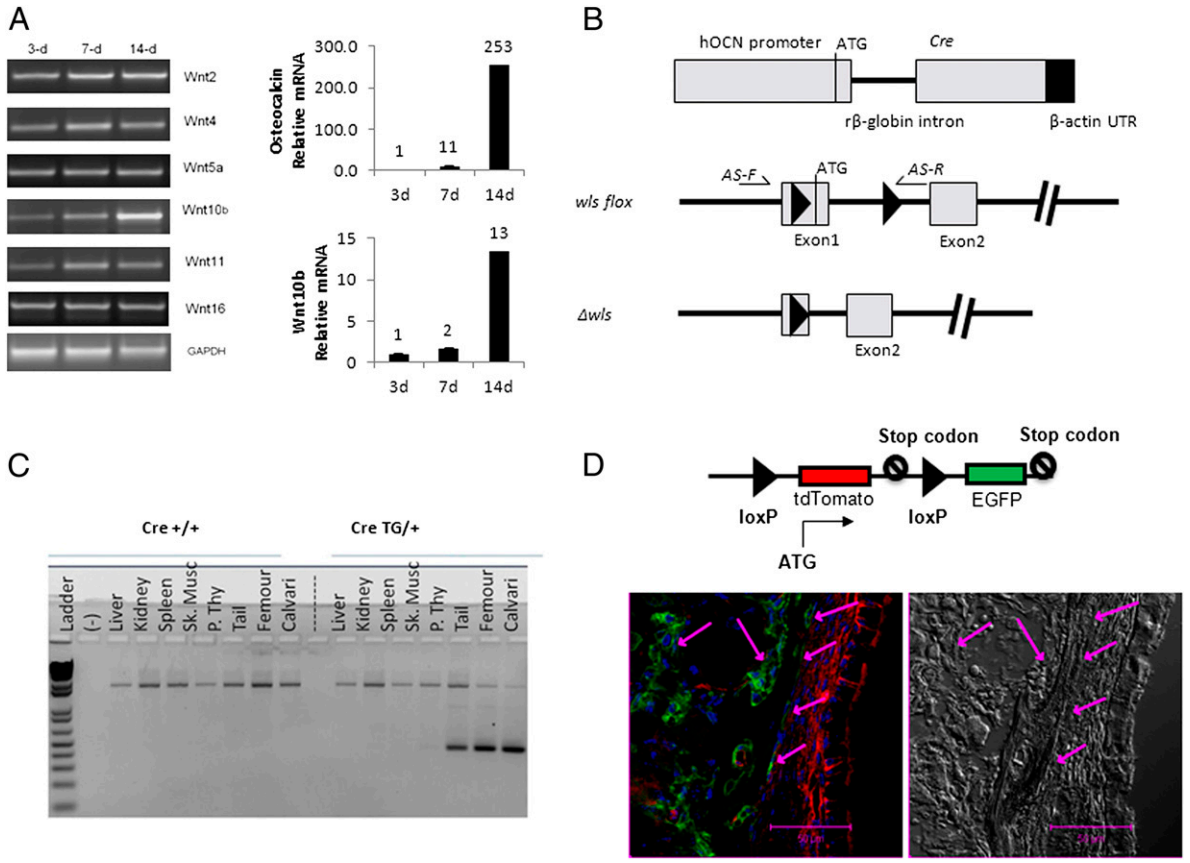

Fig. 1. Strategy and characterization of osteoblast-specific inactivation of *Wls*. (*A*) Primary calvarial cells from 3-d-old wild-type pups were differentiated to osteoblasts in osteogenic medium. Cells were collected, and RNA was extracted at the indicated time points. RT-PCR was performed to analyze the indicated Wnt gene expression profiles; GAPDH was the internal control. Real-time PCR detected the transcription of osteocalcin (a marker of osteoblast differentiation) and Wnt10b. (*B*) Human osteocalcin (hOCN) promoter was used to generate a mouse line expressing a *Cre* transgene. To generate a *Wls*-floxed allele, exon 1 (containing the ATG start codon) was flanked by two loxP sequences (black arrowheads). Cre-mediated recombination resulted in exon 1 deletion and generated the $Wls^{\Delta/\Delta}$ mutant. Primers (arrows, AS-F and AS-R) were used for allele-specific PCR to detect exon 1 deletion. (*C*) Detection of $Wls^{\Delta/\Delta}$ allele in mutant ($Cre^{TG/+};Wls^{flox/flox}$) and control ($Cre^{+/+};Wls^{flox/flox}$) mice. Allele-specific PCR using genomic DNA from different tissues generated two products representing the *Wls*-floxed allele (*Upper*) and the *Wls*-deletion allele (*Lower*). Deletion of *Wls* exon 1 was detected only in skeletal tissues. (*D*) Calvaria were collected from 1-d-old $Ocn\text{-}Cre^{TG/+};mT/mG^{KI/+}$ mice and were decalcified in 19% (wt/vol) EDTA overnight. A cryosection was prepared, stained with DAPI (blue), and observed with a fluorescence confocal microscope. The arrows indicate the bone cells expressing GFP (green). A differential interference contrast image of the same area is at right. (Scale bar, 50 μm.)

inactivated in both osteoblasts and osteocytes (because osteocytes originate from osteoblasts). Allele-specific PCR analysis with primers flanking exon 1 of *Wls* showed that Cre-mediated recombination occurred only in tissues containing bone, including the tail, femur, and calvaria (Fig. 1*C*). We further evaluated Cre activity in *Ocn-Cre* mice by crossing *Ocn-Cre* TG^+ mice with *ROSA26* (Fig. S2*A*) and *mT/mG* reporter mice and found that activity was highly specific for osteoblasts, with activity occasionally detected in a small number of hypertrophic chondrocytes (Fig. 1*D* and Fig. S3). We investigated the expression of Gpr177 in the distal femoral metaphysis by immunohistochemical analysis using the anti-mouse Gpr177 antibody. We found Gpr177 expression in the wild-type bone cells but not in the *Wls*-homozygous mutant bone cells (see Fig. 4*C*). Immunoblotting showed that Gpr177 protein expression was reduced in primary calvarial cells (a fraction of calvarial cells are mature osteoblasts) taken from *Wls*-homozygous mutant mice (Fig. S2*B*).

Osteoblast-Specific Inactivation of *Wls* Dramatically Reduces Bone Accrual. We generated cohorts of wild-type (lacking the *Ocn-Cre* gene), heterozygous ($Ocn\text{-}Cre^{TG/+};Wls^{flox/+}$), and homozygous ($Ocn\text{-}Cre^{TG/+};Wls^{flox/flox}$, referred to as "$Wls^{\Delta/\Delta}$") conditional knockout animals. As predicted by the timing of *Ocn-Cre* expression and previous studies (16), whole-mount skeletal staining did not reveal any obvious differences in embryos at embryonic day (E) 18.5 (Fig. 2*A*). In addition, we did not find any differences in 10-d-old animals either by whole-body CT scan (Fig. 2*B*) or 3D microcomputed tomography (microCT) analysis of the distal femur. However, most $Wls^{\Delta/\Delta}$ mice developed spontaneous fractures early in life, which can be seen in the whole-body CT scan (Fig. 2*C*). These fractures rendered the animals immobile and necessitated their euthanasia.

We performed a longitudinal analysis of bone mineral density (BMD) using dual-energy X-ray absorptiometry (DXA). The $Wls^{\Delta/\Delta}$ mice of both sexes displayed a significant reduction in BMD as early as 20 d of age, and these differences became even more significant as the animals aged (Fig. 2*D*). In both sexes, the body weight of $Wls^{\Delta/\Delta}$ mice was lower than that of the wild types or heterozygotes (Fig. S4*A*). Fewer than 20% of the $Wls^{\Delta/\Delta}$ mice survived to 2 mo of age (Fig. 2*E*). A few individual mice survived up to 4 mo despite extremely low bone mass.

We further characterized the low-bone-mass phenotype in 7-wk-old *Wls*-deficient mice by microCT scans of femurs (Fig. 3*A*). The ratio of bone volume to tissue volume (BV/TV) within the distal femur metaphysis in male $Wls^{\Delta/\Delta}$ mice was decreased by more than 90% compared with that of controls and hetero-

Downloaded at Palestinian Territory, occupied on November 26, 2021
www.manaraa.com

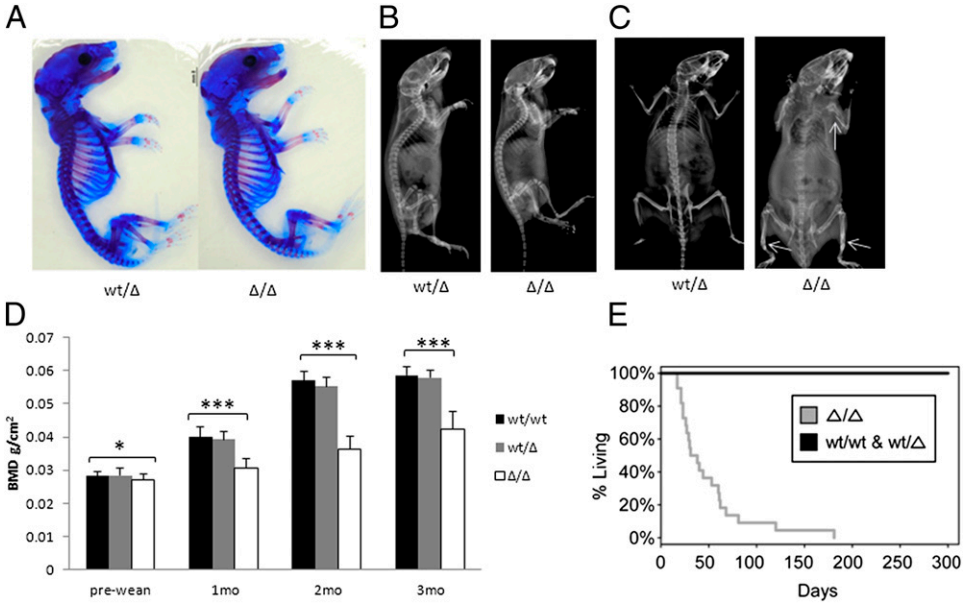

Fig. 2. Inactivation of *Wls* leads to a dramatic reduction of bone accrual. (*A*) Whole-mount skeletal staining at E18.5 shows no difference between heterozygous (WT/Δ) and homozygous (Δ/Δ) embryos. (*B* and *C*) High-resolution X-ray images of heterozygous (WT/Δ) and homozygous (Δ/Δ) mice at age 10 d (*B*) and 1 mo (*C*). No difference was observed at 10 d; arrows indicate fracture sites in the limbs of the 1-mo-old $Wls^{\Delta/\Delta}$ mouse. (*D*) Total body (excluding the skull) BMD of wild-type (WT/WT), heterozygous (WT/Δ), and *homozygous* (Δ/Δ) male mice was determined by DXA at the indicated time points. The $Wls^{\Delta/\Delta}$ mice showed a significantly lower bone density than wild types and heterozygotes after weaning (20 d of age). $^*P < 0.05$; $^{***}P < 0.001$. (*E*) Kaplan–Meier survival plot of $Wls^{\Delta/\Delta}$ mice, most of which die before 2 mo of age (log-rank test, $P = 7.173 \times 10^{-13}$).

zygotes, and the cortical bone thickness of the femur midshaft was reduced by more than 50% (Fig. 3*B*). We observed a similar change in female $Wls^{\Delta/\Delta}$ mice. Toluidine blue and von Kossa staining of the distal femur indicated that $Wls^{\Delta/\Delta}$ mice progressively lost trabecular bone and cartilage (Fig. 3*C*). The calvarial bone in $Wls^{\Delta/\Delta}$ mice also was significantly thinner (Fig. 3*A*). Thus, *Wls* inactivation in osteoblasts affects both intramembranous and endochondral bone formation.

Osteoblast-Specific Inactivation of *Wls* Inhibits Wnt/β-Catenin Signaling, Decreases Matrix Formation, and Increases Bone Resorption. Because *Wls* plays a critical role in Wnt secretion, we reasoned the low-bone-mass phenotype of $Wls^{\Delta/\Delta}$ mice resulted at least in part from defects in Wnt/β-catenin signaling. Consistent with microCT findings, histological analysis showed that $Wls^{\Delta/\Delta}$ mice had significantly less trabecular bone in both the femur and the lumbar vertebrae (Fig. 4*A* and Fig. S5*C*). Immunohistochemical analysis of sections from both the femur metaphysis and vertebral bone showed significantly reduced β-catenin staining in bone cells (Fig. 4*F* and Fig. S5*D*). To assess Wnt/β-catenin signaling further, we crossed *Ocn-Cre;Wls-flox* mice with transgenic mice carrying the β-catenin–responsive *BAT-gal* reporter gene (17). The reporter gene activity, detected by X-gal staining for β-galactosidase, was notably reduced in trabecular and cortical bone from $Wls^{\Delta/\Delta}$ mice (Fig. S1 *C* and *F*). These data suggested that a loss of *Wls* and the corresponding inability of mature osteoblasts to secrete Wnts inhibited Wnt/β-catenin signaling in the bone. Previous studies have found that deletion of β-catenin within mature osteoblasts led to increased bone resorption that was associated with changes in osteoprotegerin/receptor activator of NF-κB ligand (OPG/RANKL) signaling. Consistent with increased osteoclastic resorption activity, we observed a noted enhancement of tartrate-resistant acid phosphatase (TRAP) staining in the $Wls^{\Delta/\Delta}$ femoral growth plate (Fig. 4*H*).

To gain further insight into the loss of *Wls* in mature osteoblasts, we performed histomorphometric analysis of the distal femurs and the fifth lumbar vertebrae. There was no noticeable difference between heterozygotes and wild types. In $Wls^{\Delta/\Delta}$ mice the BV/TV ratio was reduced by half at 4 wk of age and by about 95% at 8 wk as compared with controls. The osteoblast surface (Ob.S) was reduced significantly, and the osteoclast surface (Oc.S) was increased significantly in 4-wk-old $Wls^{\Delta/\Delta}$ mice (Table 1). Although the ratio of Ob.S to bone surface (Ob.S/BS) increased dramatically in 8-wk-old $Wls^{\Delta/\Delta}$ mice, these osteoblasts appeared to be smaller and functionally deficient, because both the mineral apposition rate (MAR) and the surface-based bone formation (BFR/BS) rate were reduced substantially (Table 1 and Fig. S6). Consistent with reduced osteoblastic activity, serum osteocalcin (Ocn) in $Wls^{\Delta/\Delta}$ mice is significantly lower at both 1 mo and 2 mo of age (Fig. S4*B*). We did not detect differences in serum C-terminal telopeptides of type I collagen (CTX-I) levels in $Wls^{\Delta/\Delta}$ mice, but the level of serum C-terminal telopeptides of type II collagen (CTX-II) is elevated dramatically in $Wls^{\Delta/\Delta}$ mice (Fig. S4 *C* and *D*), indicating cartilage degradation. Collectively, these data demonstrated a decrease in bone formation and an increase in matrix resorption in mice carrying a conditional deletion of *Wls* in mature osteoblasts.

Wls-Deficient Osteoblasts Show Lower Wnt/β-Catenin Signaling and a Maturation Defect. To examine the cellular mechanisms responsible for the phenotypes seen in the $Wls^{\Delta/\Delta}$ mice, we studied the effect of *Wls* inactivation in differentiating primary osteoblasts in vitro. Calvarial cells derived from 3-d-old neonatal mice homozygous for the floxed allele of *Wls* ($Wls^{flox/flox}$) were infected with adenovirus expressing either Cre recombinase or EGFP. At 48 h after the infection, the cells were differentiated in osteogenic medium containing β-glycerol phosphate and ascorbic acid. Seventy-two hours after infection, Cre-mediated recombination was detected by allele-specific PCR, which showed the mutant *Wls* band only in the Cre-infected cells (Fig. 5*A*). Immunoblotting confirmed a dramatic reduction in Gpr177 protein expression in the Cre-infected cells (Fig. 5*B*). In addition, β-catenin protein levels were down-regulated in the Cre-infected cells (Fig. 5*B*). We did not detect significant changes in either prolifera-

Downloaded at Palestinian Territory, occupied on November 26, 2021
www.manaraa.com

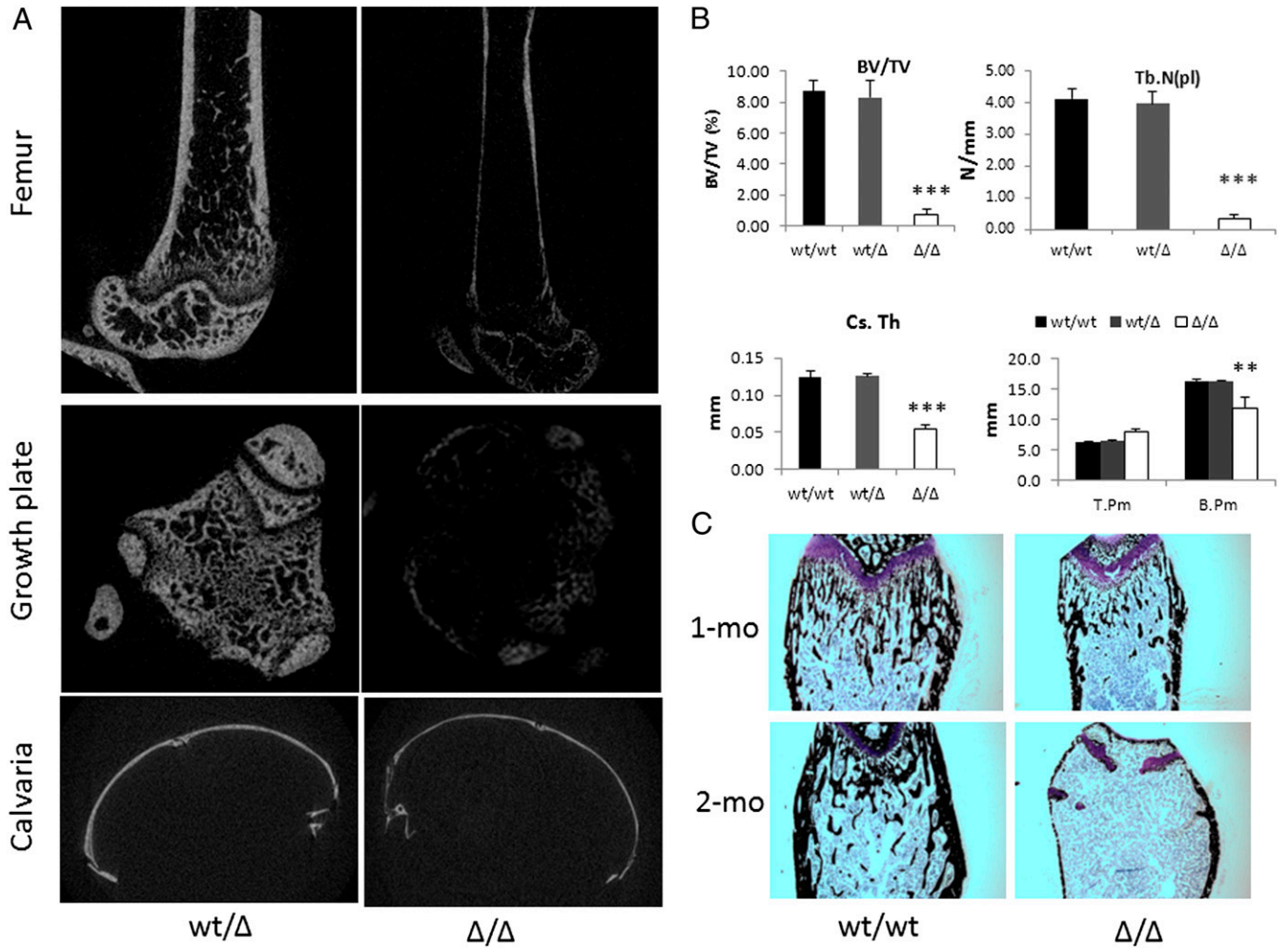

Fig. 3. MicroCT and histological analysis of osteoblast-specific *Wls*-deficient mice. (*A*) MicroCT analysis of femur and calvaria from WT/Δ and $Wls^{\Delta/\Delta}$ (Δ/Δ) mice (male, 7 wk of age). (*B*) BV/TV, trabecular number (Tb.N) of distal femoral trabecular bone, cross-sectional thickness (Cs.Th) of cortical bone in the femoral midshaft, mean total cross-sectional tissue perimeter (T. Pm), and mean total cross-sectional bone perimeter (B.Pm) were compared among the three groups. $^{**}P < 0.01$; $^{***}P < 0.001$. (*C*) Toluidine blue and von Kossa staining of the distal femoral bone from 1-mo-old and 2-mo-old male mice. The $Wls^{\Delta/\Delta}$ mice showed a progressive loss of trabecular bone. No difference was observed between WT/WT and WT/Δ mice.

tion or apoptosis in *Wls*-deficient bone cells in vitro or in vivo (Fig. S7). However, *Wls*-deficient cells showed lower alkaline phosphatase (ALP) activity after 6 d of differentiation in osteogenic medium (Fig. 5*D*). Consistent with a model in which loss of *Wls* caused low-bone-mass phenotypes because of a defect in Wnt protein secretion, the difference of ALP activity between the GFP- and Cre-infected cells could be rescued by treatment with recombinant Wnt3a (Fig. 5*D*).

The mineralization activity measured by alizarin red and von Kossa staining was reduced dramatically in Cre-infected cells (Fig. 5*E*). Using real-time PCR, we confirmed that *Axin2* transcription (a Wnt target gene commonly used as a marker for Wnt/β-catenin signaling) was decreased about fourfold, and osterix and Ocn transcription were decreased about twofold (Fig. 5*C*). The level of *Runx2*, an important transcription factor in the early stages of osteoblast differentiation, was not reduced significantly. This result is consistent with our previous findings that β-catenin–deficient and Lrp5/6-deficient osteoblasts have normal *Runx2* expression (18, 19).

Discussion

In this study, we investigated the importance of osteoblasts as Wnt-secreting cells in the bone. Using the *Ocn-Cre* driver to inactivate *Wls* conditionally, preferentially in mature osteoblasts and osteocytes, we blocked Wnt secretion from these cells and found a severe low-bone-mass phenotype associated with both decreased bone formation and increased matrix resorption. Thus, this study specifically validates the importance of Wls/Gpr177 in establishing and maintaining mouse bone mass and emphasizes the importance of functional studies to confirm the associations established by genome-wide association studies.

Given the key roles of Wnt receptors and downstream components of its signaling pathway in establishing and maintaining normal bone mass, it is not surprising that Wnt is required. However, given the many cells types within the bone microenvironment capable of secreting Wnts, it is surprising that those originating from mature osteoblasts play such a crucial role in establishing and maintaining mouse bone mass.

This work suggests that a positive feedback loop may exist within the osteoblast lineage to control the pace of differentiation of osteochondral progenitor cells, with Wnts secreted from mature cells in the lineage inducing additional osteoblast differentiation. To gain more insight into which Wnts might mediate these effects from mature osteoblasts, we examined the expression of all 19 Wnts during the course of osteoblast differentiation in vitro. Osteoblasts gradually increased transcrip-

Downloaded at Palestinian Territory, occupied on November 26, 2021
www.manaraa.com

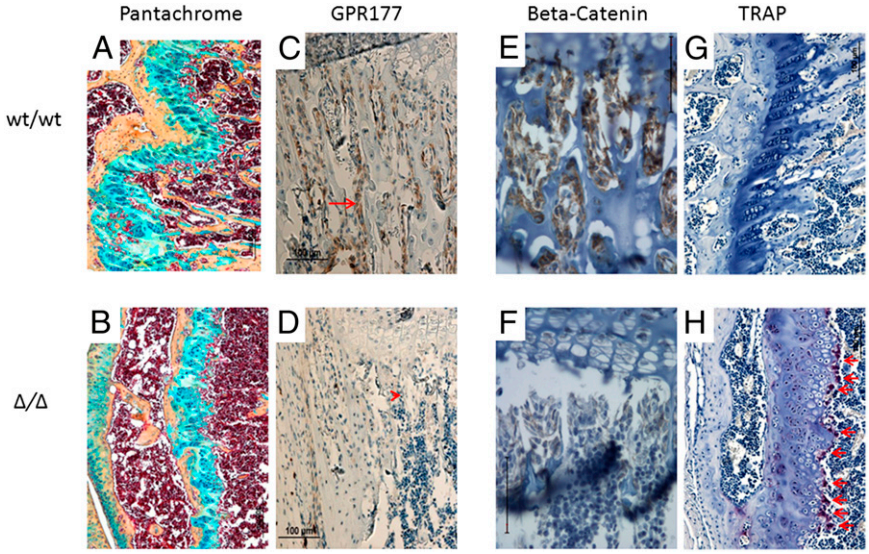

Fig. 4. Inactivation of Wls leads to inhibited Wnt/β-catenin signaling and increased osteoclast activity. (*A* and *B*) Representative pentachrome-stained images of distal femoral growth plates from 7-wk-old WT/WT (*A*) and $Wls^{\Delta/\Delta}$ (Δ/Δ) (*B*) littermates. Many fewer trabeculae were noticed in the $Wls^{\Delta/\Delta}$ growth plate. (*C*–*F*) Immunohistochemical detection of Gpr177 (*C* and *D*) and β-catenin (*E* and *F*) in the femoral metaphysis of 7-wk-old wild-type (WT/WT) and $Wls^{\Delta/\Delta}$ (Δ/Δ) littermates. Gpr177 was expressed in the wild-type bone cells (*C*, arrow) but not in $Wls^{\Delta/\Delta}$ cells (*D*, arrowhead). β-Catenin expression was decreased in $Wls^{\Delta/\Delta}$ bone cells (*F*). (*G* and *H*) Representative images of TRAP staining in the distal femoral metaphysis of 7-wk-old WT/WT (*G*) and $Wls^{\Delta/\Delta}$ (Δ/Δ) (*H*) littermates. TRAP activity is notably higher in the $Wls^{\Delta/\Delta}$ trabecular bone of growth plate (*H*, arrows). (Scale bars, 100 μm.)

tion of several Wnts as they progressed through stages of differentiation (Fig. 1*A*), with Wnt10b expression showing the strongest association with osteoblast differentiation state. Although mice with global Wnt10b inactivation ($Wnt10b^{-/-}$) have a low-bone-mass phenotype, it was much less severe than that seen in osteoblast-specific *Wls*-knockout mice, suggesting that several Wnt ligands can contribute to the phenotype we observed, as would be consistent with the increased expression of several such ligands (Fig. 1*A*). This notion also is consistent with recent work showing that Wnt6, Wnt10a, and Wnt10b are all capable of stimulating osteoblastogenesis via a β-catenin–dependent mechanism (20). In addition, β-catenin–independent targets of Wnt ligands also may contribute to the phenotypes observed (21).

Several aspects of this work show that loss of *Wls* within Ocn-cre–expressing cells leads to increased osteoclast activity. First, both histomorphometry and TRAP staining clearly show increased numbers of osteoclasts in $Wls^{\Delta/\Delta}$ mice. TRAP staining in $Wls^{\Delta/\Delta}$ mice was clearly enriched at the growth plate with little activity detected along diaphyseal cortical bone. Interestingly, TRAP staining in samples from Ocn-cre;β-catenin$^{flox/flox}$ mutant mice revealed increased osteoclast activity at both the growth plate and diaphyseal cortical bone (Fig. S8). Because $Wls^{\Delta/\Delta}$ osteoblasts have significantly reduced β-catenin signaling and because OPG is reported to be a direct β-catenin target gene (22, 23), we examined the expression of OPG and RANKL; however, we did not observe any significant decrease in the OPG/RANKL ratio (Fig. S9).

The role of Wnts in mediating interactions between osteoblasts and osteoclasts is complex and multifaceted. Aside from the role of OPG/RANKL signaling, another consideration is the recent demonstration that activation of β-catenin increases proliferation of osteoclast precursors but suppresses terminal osteoclast differentiation (24). This effect implies that decreased exposure to Wnt ligands may have stage-dependent effects on osteoclast differentiation. For example, we have observed that addition of Wnt3a to wild-type bone marrow cells in vitro inhibits osteoclastogenesis induced by macrophage colony-stimulating factor (M-CSF)/RANKL (Fig. S10*C*). Interestingly, recent studies have shown clearly that Wnt5a-induced activation of β-catenin–independent pathways within osteoclasts enhances differentiation and activity (25). Thus, we speculate that localized control of osteoclast differentiation and activity is regulated by precise combinations of Wnts with differential functions. This

Table 1. Histomorphometric indices for wild-type (WT/WT), heterozygous (WT/Δ), and $Wls^{\Delta/\Delta}$ (Δ/Δ) male mice

		Mean ± SEM						
		BV	TV	BV/TV	Ob.S/BS (%)	Oc.S/BS (%)	MAR (μm/d)	BFR/BS
8 wk	WT/WT (n = 4)	0.64 ± 0.06	3.79 ± 0.12	16.92 ± 1.42	4.5 ± 2.09	4.9 ± 1.54	2.3 ± 0.31	0.2 ± 0.05
	WT/Δ (n = 3)	0.58 ± 0.17	3.23 ± 0.4	16.14 ± 8	5.0 ± 2.32	5.3 ± 1.16	2.1 ± 0.19	0.2 ± 0.05
	Δ/Δ (n = 4)	0.02 ± 0.02***	2.56 ± 0.37**	0.91 ± 0.86***	22.3 ± 7.47**	33.4 ± 11.22**	0.6 ± 0.72**	0.0 ± 0.06**
4 wk	WT/WT (n = 4)	0.60 ± 0.13	3.60 ± 0.48	16.75 ± 2.99	38.11 ± 6.61	7.59 ± 0.68	ND	ND
	Δ/Δ (n = 3)	0.22 ± 0.03**	2.74 ± 0.66	8.43 ± 1.07**	22.15 ± 9.08*	12.51 ± 3.58*	ND	ND

Measurements are from the distal femurs of 4-wk-old mice and the fifth lumbar vertebrae of 8-wk-old mice. Values shown are mean ± SD. ND, not determined.
*$P < 0.05$ (compared with WT/WT).
**$P < 0.01$ (compared with WT/WT).
***$P < 10^{-6}$ (compared with WT/WT).

Downloaded at Palestinian Territory, occupied on November 26, 2021
www.manaraa.com

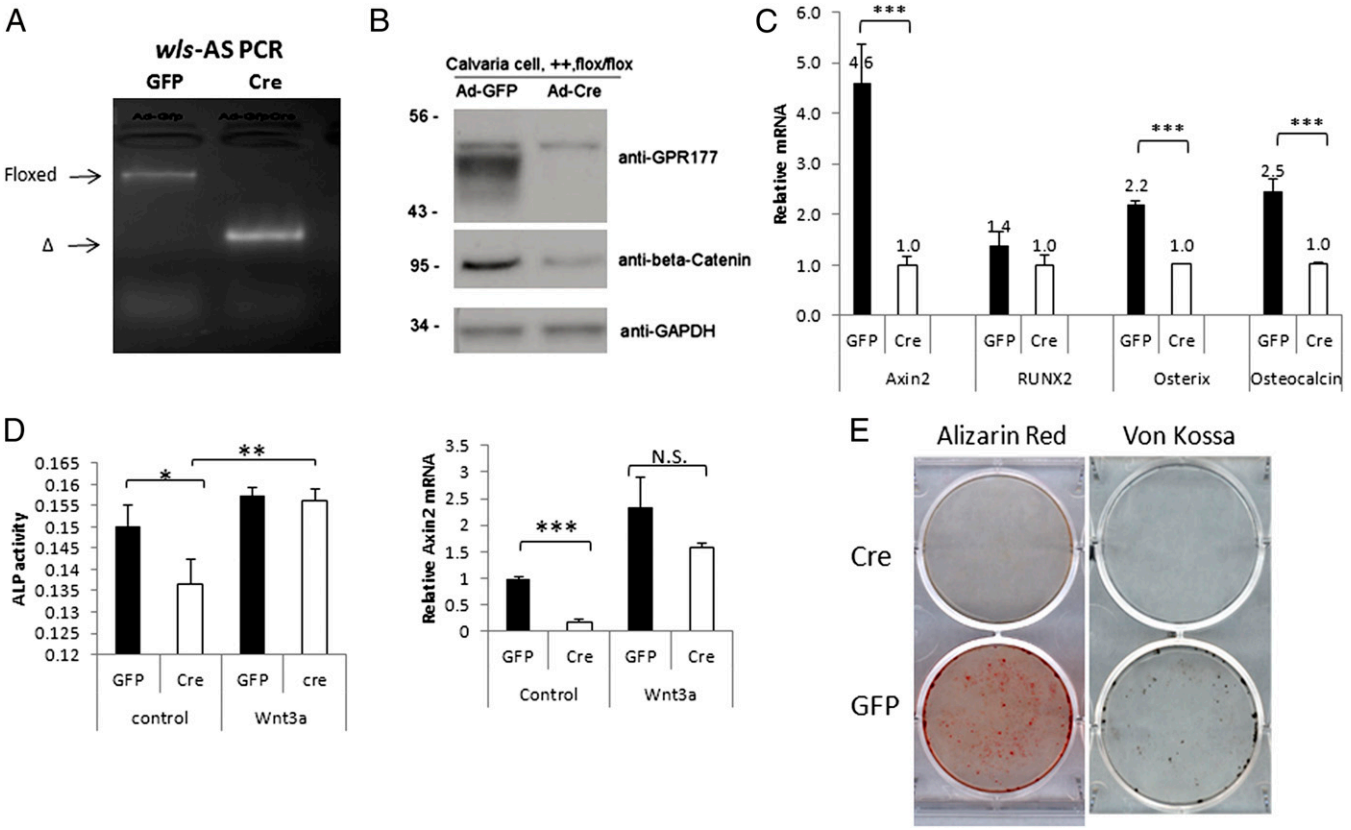

Fig. 5. Inactivation of *Wls* in osteoblasts in vitro reduces Wnt/β-catenin signaling and inhibits osteoblast differentiation. (*A*) Allele-specific PCR detection of the *Δ/ΔWls* allele in primary $Wls^{flox/flox}$ calvarial cells infected by adenovirus expressing either GFP or Cre. The *Δ/ΔWls* band (Δ) was observed only in the Cre-infected sample. (*B*) Immunoblotting of primary $Wls^{flox/flox}$ calvarial cells infected by adenovirus expressing GFP (Ad-GFP) or Cre (Ad-Cre). Whole-cell lysates from the osteoblasts were collected 48 h after infection. Immunoblotting was performed with anti-Gpr177 and anti–β-catenin antibodies; GAPDH was the loading control. The Gpr177 protein was almost absent in Cre-infected cells (a nonspecific band was observed above Gpr177 band). β-Catenin was down-regulated dramatically in Cre-infected cells. (*C*) Real-time PCR using the RNA from $Wls^{flox/flox}$ calvarial cells infected with either GFP or Cre and differentiated in osteogenic medium for 14 d. (*D*) (*Left*) ALP activity of the primary $Wls^{flox/flox}$ calvarial cells infected with GFP or Cre was determined after 7-d differentiation with or without recombinant Wnt3a treatment. RNA was extracted 24 h after Wnt3a treatment. (*Right*) Real-time PCR was used to detect Axin2 expression. (*E*) Representative images of alizarin red and von Kossa staining. The $Wls^{flox/flox}$ calvarial cells were infected by either GFP or Cre and then were differentiated in osteogenic medium for 14 d. $*P < 0.05$; $**P < 0.01$; $***P < 10^{-3}$.

complexity could explain our inability to recapitulate the elevated osteoclastogenesis using in vitro differentiation models with Wls-deficient osteoblasts or bone marrow cells from $Wls^{\Delta/\Delta}$ mice (Fig. S10). The assessment of how these signals are integrated to coordinate osteoclast activity will be a crucial area of future study.

Loss of *Wls* results in the inability to secrete Wnt proteins from the cell (26), potentially leading these proteins to accumulate in the secretory pathway, where this accumulation could lead to induction of an endoplasmic reticulum (ER) stress response similar to the unfolded protein response (27). However, the ER stress response has been shown to be required for and capable of promoting osteoblast differentiation (28, 29). Thus, given that loss of *Wls* is associated with low bone mass in vivo and impaired osteoblast differentiation in vitro, we believe it is unlikely that an ER stress response contributes to the phenotypes we have observed.

In summary, our findings reveal a critical role for mature osteoblasts as Wnt-secreting cells in bone. Inhibition of Wnt secretion from mature osteoblasts and osteocytes leads to both decreased bone formation and increased matrix resorption. These data support a strong association between SNPs within *Wls*/*Gpr177* and bone-mass accrual, and the low-bone-mass phenotype may be caused by actions of this gene within mature osteoblasts to control the secretion of Wnts. Finally, this information is important in considering the potential side effects of clinical agents that interfere with the production of Wnts. For example, the inhibition of Porcupine activity, which also is required for Wnt secretion, is being developed as an agent to treat several types of tumors (reviewed in ref. 30). Patients being treated with such agents may benefit from enhanced screening for and awareness of the possibility of reduced bone mass and increased fracture risk.

Materials and Methods

Mouse Lines. A targeting vector (Fig. 1*B*) designed to replace part of the first coding exon of the *Wls* gene with a selectable marker was used to create a strain of mice carrying a conditional null allele of *Wls* at R.A.L.'s laboratory. Human *Ocn-Cre*, *mT/mG*, *ROSA26*, and *BAT-gal* transgenic mice were from Jackson Laboratories and were kept in the Van Andel Research Institute Mutant Mouse Repository. The *mT/mG* reporter mouse possesses *loxP* sites at both sides of a tdTomato(mT) cassette and expresses red fluorescence in all tissues. When bred to Cre-expressing mice, the resulting offspring have the mT cassette deleted in the Cre-expressing tissues, allowing expression of the EGFP (mG) cassette located just downstream of mT. Genomic DNA was prepared from tail biopsies using an AutoGenprep 960 automated DNA isolation system (AutoGen). PCR-based strategies then were used to genotype the mice (details are available upon request). All experiments were done in compliance with the *Guidelines for the Care and Use of Animals for Scientific Research* (31). In addition, before use, all procedures were approved by the Institutional Animal Care and Use Committee of the Van Andel Research Institute.

Downloaded at Palestinian Territory, occupied on November 26, 2021
www.manaraa.com

DXA. Mice were anesthetized by inhalation of 2% (vol/vol) isoflurane (TW Medical Veterinary Supply) with oxygen (1.0 L/min) for 10 min before and during the imaging procedure (≤5 min). The mice were placed on a specimen tray in a PIXImus II bone densitometer (GE Lunar) for imaging. BMD was calculated by the PIXImus software based on the active bone area in the subcranial region within the total body image.

Radiography and microCT Analysis. The whole-body radiographs were taken with a PixArray 100 radiographic imaging system (Bioptix Inc.) using standardized settings (31 kV for 9 s). Trabecular and cortical bone architecture were assessed at the distal femoral metaphysis and femoral midshaft, respectively, using a desktop SkyScan 1172 microCT imaging system (SkyScan N.V.). Scans were acquired using a 6.3-μm^3 isotropic voxel size, with 300 CT slices evaluated at the distal femur and 200 CT slices at the femoral midshaft. For trabecular and cortical bone analyses, fixed thresholds of 96 and 142, respectively, were used to determine the mineralized bone fraction. Individual CT slices were reconstructed with SkyScan reconstruction software, and data were analyzed with CTan. The region of interest of trabecular bone was drawn manually a few voxels away from the endocortical surface. 3D analysis was used for trabecular bone, and 2D analysis was used for cortical bone.

Bone Histomorphometry. All mice received s.c. injections of calcein (10 mg/kg) at 8 and 3 d before they were killed. Bone samples were dissected and fixed in 4% paraformaldehyde. The distal femurs or fifth lumbar vertebral bodies were dehydrated in graded concentrations of ethanol and xylene and were embedded undecalcified in methyl methacrylate for sectioning with a Leica RM 2265 microtome (Leica Microsystems Nussloch GmbH) into 4- and 8-μm-thick sections. The 8-μm sections were left unstained for measurement of surface-based histomorphometric indices using an Eclipse E400fluorescent microscope (Nikon) linked to image analysis software (Bioquant Image Analysis Corporation). The 4-μm sections were stained with toluidine blue to measure bone volume, architecture, Ob.S, and Oc.S with a light microscope. These indices were used to calculate Ob.S/BS, Oc.S/BS, MAR, and BFR/BS at the trabecular surfaces.

Immunohistochemistry and Serum Bone Biomarkers. Bone tissue samples were fixed in 4% paraformaldehyde and decalcified in 10% EDTA for 5–10 d. Tissues were paraffin- or OCT-embedded, and 7-μm sections were adhered to glass slides. Immunohistochemistry was done by Ventana Medical System with the antibodies β-catenin (Cell Signaling) or Gpr177 (provided by R.A.L.). TRAP staining of osteoclasts was performed using a leukocyte acid phosphate kit (Sigma) with fast red violet. The apoptosis detection based on TUNEL technology used an in situ cell-death detection kit with diacetylbenzene (DAB) (Roche Applied Science). The fluorescent signal in mT/mG cryosectioned tissues was detected using a Zeiss confocal microscope. ELISA or enzyme-linked immunosorbent assay was used to determine serum biomarkers for CTX-1 (AC-06F1) (IDS), CTX-2 (AC-08F1) (IDS), Ocn (BT-470) (Biomedical Technologies Inc.), OPG (MOP00) (R&D Systems), and RANKL (MTR00) (R&D Systems).

Quantitative Real-Time RT-PCR Analysis. Total RNA was extracted from cells using RNeasy (Qiagen). The extracted RNA was used for cDNA synthesis via reverse transcriptase using SuperScript III and random primers (Invitrogen). The cDNA samples were subjected to PCR analysis using Taqman PCR Master Mix and 20× primer and probes (Applied Biosystems). Amplifications then were performed on an ABI 7500 Real-time PCR system. The expression of the gene of interest and the housekeeping gene (18S ribosomal RNA) were determined simultaneously in the same sample. For each sample, mRNA levels for each gene were normalized to 18s rRNA levels. The Wnt expression profile was determined by RT-PCR using the same primer sets used for the reference (14).

Osteoblast Isolation and Culture. Osteoblasts were isolated from calvaria of newborn $Wls^{flox/flox}$ mice by serial digestion in 0.2 mg/mL collagenase type I (Worthington). In short, calvaria were digested for 15 min at 37 °C with constant agitation. The digestion solution was collected and digested an additional five times. Digestions 3–6 (containing the osteoblasts) were centrifuged, washed with α-MEM (Eagle's minimum essential medium) containing 10% FBS and 1% (wt/vol) penicillin/streptomycin, and cultured for 48 h at 37 °C. For the in vitro Wnt3a treatment, cells were incubated in medium containing 80 ng/mL of recombinant Wnt3a (R&D Systems) for 8 h, after which the medium was replaced with fresh medium without Wnt3a. Osteoblasts grown in monolayer were infected with control adenovirus (Ad-GFP) or Cre-recombinase virus (Ad-Cre) (Microbix Biosystems) at a multiplicity of infection of 150 for most experiments. Osteoblasts were harvested and plated to six-well plates after 48 h. Osteoblasts were differentiated in osteogenic medium (change every 2 d) containing 50 μg/mL ascorbic acid and 10 mM β-glycerol phosphate. ALP staining was done with One-Step NBT-BCIP (catalog no. 34042; Thermo Scientific). For quantification of ALP activity, the cell lysate was incubated with One-Step NBT-BCIP solution at 37 °C and read at 570 nm. A BCA assay (Pierce) was performed to detect the protein concentration. von Kossa staining and alizarin red staining used 3% (wt/vol) silver nitrate in distilled water and 40 mM alizarin red S solution, respectively.

Bone Marrow Cell Isolation and Osteoclast Cultures. Bone marrow cells were isolated by flushing femurs from 4-wk-old male mice. Osteoclast-like cells were generated by plating the bone marrow cells at 2×10^6 cells per well in 24-well plates in differentiation medium: α-MEM supplemented with 10% (vol/vol) FBS, M-CSF (40 ng/mL), and RANKL (100 ng/mL).

Bone Resorption Assay. Bone marrow cells were isolated as described above and plated in Corning Osteo Assay Surface 24-well plates (Corning Life Sciences), which are built with inorganic bone biomaterial surface. Medium and treatments were changed every 3 d until the end of a 14-d culture period. Wells were stained with von Kossa solution (5% [wt/vol] aqueous silver nitrate). The unresorbed mineralized surface turns black, and the resorbed areas are white. Three wells were assessed for each group.

Statistical Analyses. Results are presented as mean ± SD, with n equal to the number of samples analyzed. ANOVA or the Student's t test was used to test for significant differences between data sets. Significance was defined as $P < 0.05$.

ACKNOWLEDGMENTS. We thank members of the Williams laboratory and other members of the Van Andel Research Institute Center for Skeletal Disease Research for advice and assistance, Drs. Steven Goldring and Edward Purdue for assistance with data analysis, and David Nadziejka for assistance with technical editing of this article. This work was supported by National Institutes of Health Grants AR053293 (to B.O.W.), K24-AR04884 (to N.E.L.), and AR043052 (to N.E.L.).

1. Uitterlinden AG, et al. (2004) Polymorphisms in the sclerosteosis/van Buchem disease gene (SOST) region are associated with bone-mineral density in elderly whites. *Am J Hum Genet* 75:1032–1045.
2. Gong Y, et al.; Osteoporosis-Pseudoglioma Syndrome Collaborative Group (2001) LDL receptor-related protein 5 (LRP5) affects bone accrual and eye development. *Cell* 107: 513–523.
3. Boyden LM, et al. (2002) High bone density due to a mutation in LDL-receptor-related protein 5. *N Engl J Med* 346:1513–1521.
4. Styrkarsdottir U, et al. (2009) New sequence variants associated with bone mineral density. *Nat Genet* 41:15–17.
5. Rivadeneira F, et al.; Genetic Factors for Osteoporosis (GEFOS) Consortium (2009) Twenty bone-mineral-density loci identified by large-scale meta-analysis of genome-wide association studies. *Nat Genet* 41:1199–1206.
6. Hsu YH, et al. (2010) An integration of genome-wide association study and gene expression profiling to prioritize the discovery of novel susceptibility Loci for osteoporosis-related traits. *PLoS Genet* 6:e1000977.
7. Styrkarsdottir U, et al. (2010) European bone mineral density loci are also associated with BMD in East-Asian populations. *PLoS ONE* 5:e13217.
8. Bänziger C, et al. (2006) Wntless, a conserved membrane protein dedicated to the secretion of Wnt proteins from signaling cells. *Cell* 125:509–522.
9. Bartscherer K, Pelte N, Ingelfinger D, Boutros M (2006) Secretion of Wnt ligands requires Evi, a conserved transmembrane protein. *Cell* 125:523–533.
10. Fu J, Jiang M, Mirando AJ, Yu HM, Hsu W (2009) Reciprocal regulation of Wnt and Gpr177/mouse Wntless is required for embryonic axis formation. *Proc Natl Acad Sci USA* 106:18598–18603.
11. Ching W, Hang HC, Nusse R (2008) Lipid-independent secretion of a Drosophila Wnt protein. *J Biol Chem* 283:17092–17098.
12. Kim JB, et al. (2007) Bone regeneration is regulated by wnt signaling. *J Bone Miner Res* 22:1913–1923.
13. Pederson L, Ruan M, Westendorf JJ, Khosla S, Oursler MJ (2008) Regulation of bone formation by osteoclasts involves Wnt/BMP signaling and the chemokine sphingosine-1-phosphate. *Proc Natl Acad Sci USA* 105:20764–20769.
14. Etheridge SL, Spencer GJ, Heath DJ, Genever PG (2004) Expression profiling and functional analysis of wnt signaling mechanisms in mesenchymal stem cells. *Stem Cells* 22:849–860.
15. Carpenter AC, Rao S, Wells JM, Campbell K, Lang RA (2010) Generation of mice with a conditional null allele for Wntless. *Genesis* 48:554–558.
16. Zhang M, et al. (2002) Osteoblast-specific knockout of the insulin-like growth factor (IGF) receptor gene reveals an essential role of IGF signaling in bone matrix mineralization. *J Biol Chem* 277:44005–44012.

PNAS PLUS
CELL BIOLOGY
Downloaded at Palestinian Territory, occupied on November 26, 2021
www.manaraa.com

17. Maretto S, et al. (2003) Mapping Wnt/beta-catenin signaling during mouse development and in colorectal tumors. *Proc Natl Acad Sci USA* 100:3299–3304.
18. Holmen SL, et al. (2005) Essential role of beta-catenin in postnatal bone acquisition. *J Biol Chem* 280:21162–21168.
19. Joeng KS, Schumacher CA, Zylstra-Diegel CR, Long F, Williams BO (2011) Lrp5 and Lrp6 redundantly control skeletal development in the mouse embryo. *Dev Biol* 359: 222–229.
20. Cawthorn WP, et al. (2011) Wnt6, Wnt10a and Wnt10b inhibit adipogenesis and stimulate osteoblastogenesis through a beta-catenin-dependent mechanism. *Bone*.
21. Tu X, et al. (2007) Noncanonical Wnt signaling through G protein-linked PKCdelta activation promotes bone formation. *Dev Cell* 12:113–127.
22. Glass, DA, 2nd, et al. (2005) Canonical Wnt signaling in differentiated osteoblasts controls osteoclast differentiation. *Dev Cell* 8:751–764.
23. Kramer I, et al. (2010) Osteocyte Wnt/beta-catenin signaling is required for normal bone homeostasis. *Mol Cell Biol* 30:3071–3085.
24. Wei W, et al. (2011) Biphasic and dosage-dependent regulation of osteoclastogenesis by β-catenin. *Mol Cell Biol* 31:4706–4719.
25. Maeda K, et al. (2012) Wnt5a-Ror2 signaling between osteoblast-lineage cells and osteoclast precursors enhances osteoclastogenesis. *Nat Med* 18:405–412.
26. Port F, Basler K (2010) Wnt trafficking: New insights into Wnt maturation, secretion and spreading. *Traffic* 11:1265–1271.
27. Diehl JA, Fuchs SY, Koumenis C (2011) The cell biology of the unfolded protein response. *Gastroenterology* 141(1):38–41, 41 e1–e2.
28. Tohmonda T, et al. (2011) The IRE1α-XBP1 pathway is essential for osteoblast differentiation through promoting transcription of Osterix. *EMBO Rep* 12:451–457.
29. Saito A, et al. (2011) Endoplasmic reticulum stress response mediated by the PERK-eIF2(alpha)-ATF4 pathway is involved in osteoblast differentiation induced by BMP2. *J Biol Chem* 286:4809–4818.
30. Rey JP, Ellies DL (2010) Wnt modulators in the biotech pipeline. *Dev Dyn* 239:102–114.
31. National Advisory Committee for Laboratory Animal Research (2004) *Guidelines on the Care and Use of Animals for Scientific Purposes*. Available at http://www.ava.gov.sg/NR/rdonlyres/C64255C0-3933-4EBC-B869-84621A9BF682/13557/Attach3_AnimalsforScientificPurposes.PDF.

Downloaded at Palestinian Territory, occupied on November 26, 2021

www.manaraa.com